Gu, Chao; Lyu, Ziyu; Liu, Xin; Bao, Yanping; Li, Hong; Kang, Wei; Chu, Jianhua; Lian, Junhe

Experimental and density functional theory studies on size-dependent adsorption behavior of CaO nanoparticles on Al2O3 in liquid steel

Published in:
Journal of Materials Research and Technology

DOI:
10.1016/j.jmrt.2022.08.164

Published: 01/09/2022

Document Version
Publisher's PDF, also known as Version of record

Available online at www.sciencedirect.com

jmr&t Journal of Materials Research and Technology

journal homepage: www.elsevier.com/locate/jmrt

Short Communication

Experimental and density functional theory studies on size-dependent adsorption behavior of CaO nanoparticles on Al_2O_3 in liquid steel

Chao Gu [a], Ziyu Lyu [a], Xin Liu [a], Yanping Bao [a,*], Hong Li [b], Wei Kang [b], Jianhua Chu [a], Junhe Lian [c]

[a] State Key Laboratory of Advanced Metallurgy, University of Science and Technology Beijing, Beijing, 100083, China
[b] Technology Center, Angang Steel Company Limited, Anshan, 114003, China
[c] Department of Mechanical Engineering, Aalto University, Puumiehenkuja 3, Espoo, 02150, Finland

ARTICLE INFO

Article history:
Received 29 March 2022
Accepted 29 August 2022
Available online 6 September 2022

Keywords:
In-situ experiment
Density functional theory
Adsorption
Nanoparticles
Inclusions

ABSTRACT

The properties of particles in nano-scale has been found significantly different, whereas the reaction mechanisms and adsorption behaviors of nanoparticles in liquid steel under high temperature are still not fully clarified due to the experimental difficulties. In this study, in-situ experiments and density functional theory calculations were adopted to reveal the differences of adsorption phenomenon between Al_2O_3 inclusions and CaO particles of different sizes. It is concluded that the adsorption speed and bond strength between CaO and Al_2O_3 are both larger for CaO with smaller sizes. The surface of Al_2O_3 will become rough due to chemical adsorption of CaO, encouraging more Ca atoms to participate in the adsorption and thus accelerating the adsorption process. This work presents a new insight into the reactions concerning inclusion modification in liquid steel in nano-scale and also help create opportunities for the application of nano-materials in high-efficient smelting.

1. Introduction

The physical and chemical properties of nanoparticles have been found extremely different, such as strength, diffusivity, catalytic activity, and reactive activity [1–3]. The strongly size-related behaviors provide opportunities for revolutionary innovations in both scientific and industrial technology, even in traditional industries, for instance, smelting and purification of steel. With the development of industrial society, the demand for the service performance of steel for engineering structures in various industrial sectors, e.g., aerospace, high-speed railway, automotive, etc., has steadily increased. To obtain satisfying properties of engineering materials, inhomogeneous microstructures and micro-defects existing in materials have been significantly studied through various methods [4,5]. Inclusions, as unavoidable defects, are one of the main types of research focuses [6–8]. The inclusions in

* Corresponding author.
E-mail addresses: baoyp@ustb.edu.cn, 15210951549@sina.cn (Y. Bao).
https://doi.org/10.1016/j.jmrt.2022.08.164

steel are usually formed during the deoxidation process. Researchers have conducted multiple studies on the removal of inclusions. However, inclusions, such as Al_2O_3, still cannot be eliminated in steels. Therefore, it is important to change the inclusion types to those with minimum effects on the service properties besides simple size control, which is known as the inclusion modification process [9–11]. Most of the inclusion modifications in liquid steels are dependent on the reactions between inclusions and modifying elements, such as Ca, Ba, etc. The traditional addition methods of these elements are mainly with alloy wire feeding [12–14]. The alloy wires containing modifying elements are fed into the ladle with a feeding machine to decrease the burning loss of the modifying elements. During the feeding, the mixing efficiency of the modifying elements in the furnace and the modification efficiency of inclusions are strongly determined by the flow of the molten steel and the melting property of the wires. However, the improvements in terms of these two aspects are limited by the equipment and raw materials of the wires.

To further increase the modification efficiency, small particles with modifying elements were trying to be injected into the molten steel to decrease the melting difficulty of the monolithic alloy materials [15,16]. In these studies, particle sizes were reduced to centimeter scale. Improvements in modification effects and purification of liquid steel with the decrease of particle sizes have been confirmed compared with wire feeding. Nevertheless, it is still not clarified in the existing studies how the modification efficiency and the reaction mechanism will change if the particle size keeps decreasing to micro- and nano-scale, although there are already some reports on the addition method of nano-CaO in liquid steel with high temperature [17,18].

Motivated by the above backgrounds, the aim of this study is to investigate the absorption behavior and reaction mechanism between nano-CaO particles, which is referred as a modification agent, and Al_2O_3 inclusions in liquid steel under 1550 °C. In-situ experiments are conducted to observe the motion behavior of CaO particles with different sizes under the influence of Al_2O_3 inclusions with high-temperature confocal laser scanning microscopy (HT-CLSM). Density functional theory (DFT) calculations were adopted to provide new insight into the corresponding adsorption behaviors and mechanism in liquid steel.

2. Methodology

2.1. Experimental

In the in-situ experiments, the mixed particles of CaO and Al_2O_3 were pre-set on the top surface of a steel bar with 7 mm diameter and 3 mm height with an atom ratio of 1:2 (Fig. 1(a)). The main composition of the steel bar is shown in Table 1. The particle sizes and morphologies under scanning electron microscope (SEM) of CaO and Al_2O_3 are shown in Fig. 1(b_1)-(b_2) and (c_1)-(c_2). The sizes of Al_2O_3 particles are in the range of 17.7–95.7 μm. The sizes of CaO particles are in the range of 0.39–4.38 μm. The steel bar was placed in a platinum crucible and heated. The heating rate was kept at 500 °C/min until the temperature reached 1550 °C, which is around the melting point of the steel bar. Afterwards, the temperature was artificially adjusted around 1550 °C with a fluctuation of 5 °C. Thus, only the top surface of the steel bar can be melted while the lower part kept in a solid state. The liquid surface can offer a satisfying condition for particles to move freely and limit the moving area at the same time to avoid the effect of large liquid flow.

2.2. Theoretical

For deeper insight into the adsorption behaviors under the influences of particle sizes, corresponding DFT calculations

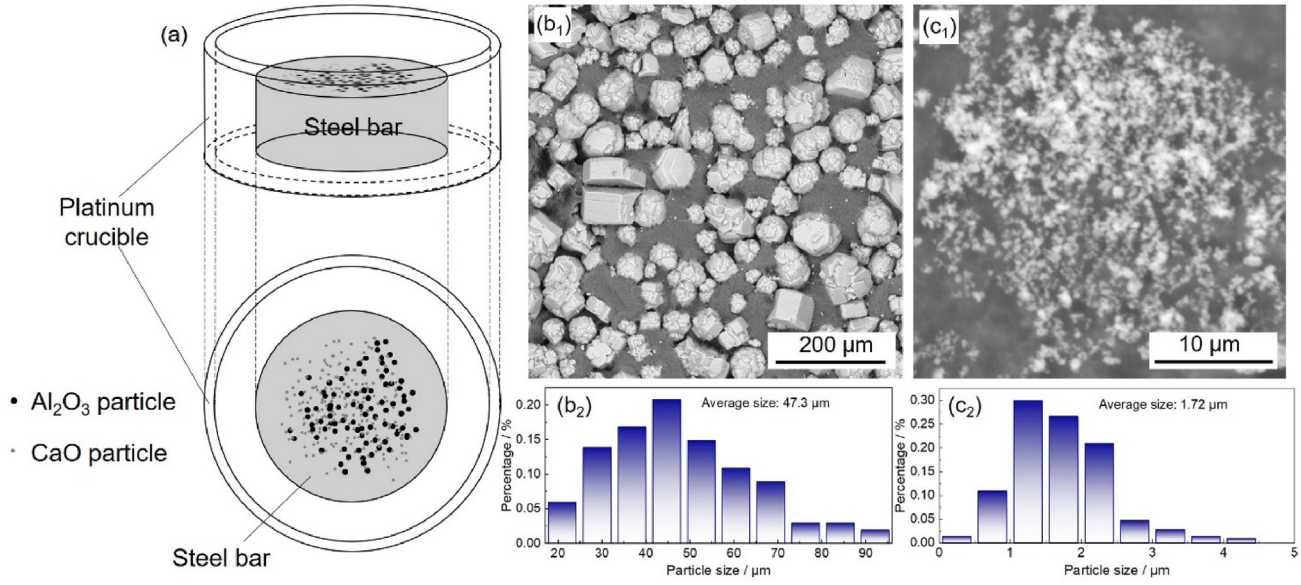

Fig. 1 – (a) Schematic illustration of samples in in-situ experiments (b_1)-(b_2) SEM morphology and size of Al_2O_3 particles (c_1)-(c_2) SEM morphology and size of CaO particles.

Table 1 – The main composition of the steel bar (unit: weight %).

C	Cr	Si	Mn	P	S	Cu	Al
1.00	1.31	0.20	0.34	0.010	0.0007	0.08	0.01

were conducted. The DFT calculations were performed with the CASTEP [19] module of Material Studio software. During the calculation, the molecular orbitals were expanded by plane wave bases. The number of plane wave bases was controlled by the level of truncation energy, which was 489.8 eV in this study. Generalized Gradient Approximation (GGA) Scheme and Perdew–Burke–Ernzerhof (PBE) [20] functional were used to describe the exchange and correlation interactions. Ultra-soft pseudopotential [21] was used to describe the interactions between electrons and ionic cores. The self-consistent process was based on whether the energy and charge density distribution of the system converge. The energy was converged with $1 \times 1 \times 1$ k point. The self-consistent field (SCF) convergence standard was set as energy change less than 2×10^{-6} eV/atom. The adsorption system was set inside a $9.5 \times 13.0 \times 27.4$ Å^3 periodic box with three parts: Fe, CaO, and Al_2O_3. CaO with different atom numbers was inserted inside the model of Fe. The model of Al_2O_3 was fixed in the bottom of the box below the model of Fe. The crystal structure of Fe was set as $a = b = c = 2.8664$ Å. In the model of Fe, other elements, such as C, Si, Cr, Mn, etc., and their effects on the reaction between CaO and Al_2O_3 were neglected due to their low contents in the steel. The ground state contained 2 atoms, based on which a supercell of 75 atoms was established. To insert CaO, atoms were removed to make room for CaO. The crystal structure of Al_2O_3 was set as $a = b = 4.759$ Å, $c = 12.991$ Å. Al_2O_3 (0 0 1) is a typical surface that can effectively describe the adsorption behavior, especially for metal atoms [22,23]. Therefore, (0 0 1) was set as the contact surface with Fe and CaO. In this system, the model with 12 Al_2O_3 was built with a vacuum layer of 22 Å on the top. Afterwards, the system was relaxed at 1550 °C under NVT (Number of particles, System Volume, Temperature) ensemble for 1 ps.

3. Results and discussion

As observed in the in-situ experiment, the adsorption process between CaO and Al_2O_3 happened fast when the top surface of the steel was melted and the particles can move freely in the liquid steel. Multiple CaO particles gradually gathered around Al_2O_3 after the adsorption behavior began. During the adsorption, Al_2O_3 with a larger size barely moved in all the observation areas, while the movement of CaO particles can be easily observed. Most of the CaO particles were strongly attracted and moved towards the Al_2O_3 particles. Complex oxides of Al–Ca–O were thus generated with thick layers of CaO outside the Al_2O_3 particles. Fig. 2(a_1)-(a_5) and Fig. 2(b_1)-(b_5) show the moving behaviors of CaO particles with sizes of 2.2 μm and 24.7 μm, respectively. The CaO particle with a larger size in Fig. 2(b_1) is a loose cluster rather than a solid chunk, which was generated due to the aggregation of small CaO particles. It is interesting to be noted that the moving speeds of CaO particles with different sizes were distinctly different (Fig. 2(c)), which are 5.5 μm/s for CaO with the size of 2.2 μm and 2.2 μm/s for CaO with the size of 24.7 μm. It can be concluded that CaO particles are easy to agglomerate with each other if there are no Al_2O_3 particles around. Once the loose clusters of CaO generate, it is more difficult to be adsorbed by Al_2O_3 compared to a single CaO particle.

According to the DFT calculations, the systems containing Fe, CaO, and Al_2O_3 before and after the adsorption are shown in Fig. 3. It is found that the Ca atom obviously moved towards the Al–O system. Adsorption happened between Al_2O_3 and CaO with different atom numbers. Distinct structure variations were observed on both Al_2O_3 and CaO. The surface of Al_2O_3 became rugged with Ca atom trapped in the dent, suggesting the adsorption was chemisorption and the Ca atom was the reaction center. The chemical bond around the Ca atom will be discussed later. Furthermore, the rugged surface will encourage more atoms to participate in the adsorption, which is one of the reasons that the adsorption process happened fast as observed in the in-situ experiment.

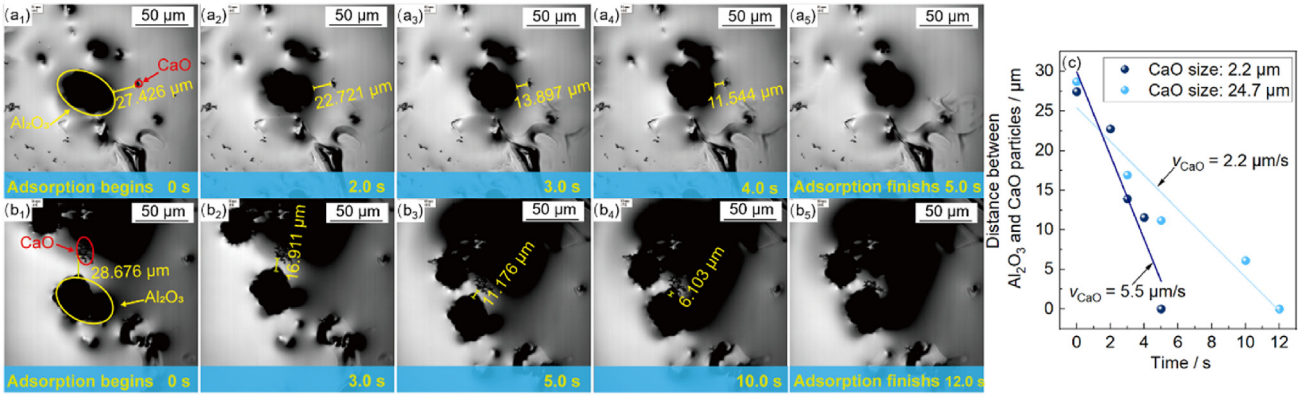

Fig. 2 – (a_1)-(a_5) moving behaviors of CaO particle (2.2 μm) (b_1)-(b_5) moving behaviors of CaO particle (24.7 μm); (c) distance variation between Al_2O_3 and CaO of different sizes.

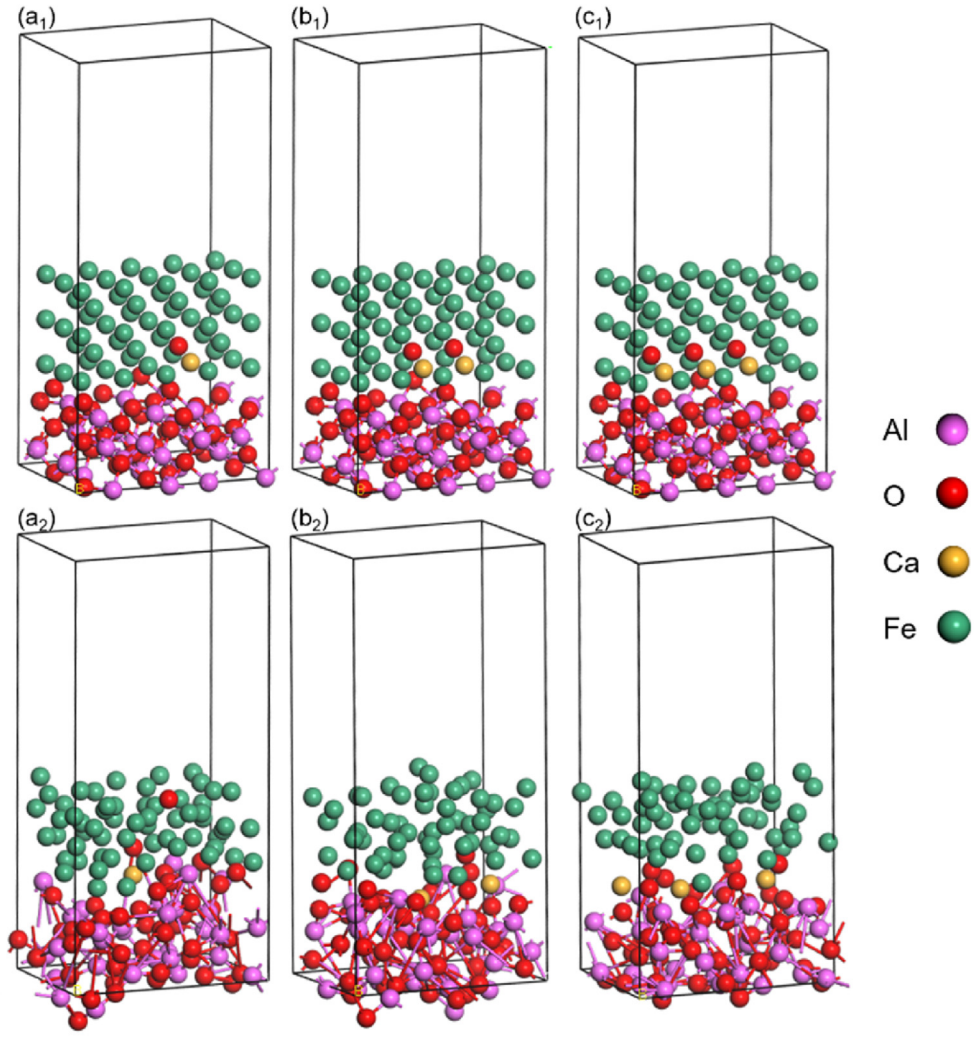

Fig. 3 – Structures before adsorption and after adsorption with CaO of different atom numbers: (a_1)-(a_2) single Ca atom (b_1)-(b_2) double Ca atoms (c_1)-(c_2) triple Ca atoms.

To compare the adsorption process of CaO with different atom amounts, the adsorption energies were calculated with Eq. (1).

$$E_{ads} = E_{tol}\text{-}(E_{slab} + E_{up}) \quad (1)$$

where E_{ads} is the adsorption energy; E_{tol} is the total energy after the adsorption; E_{slab} is the energy of the Al_2O_3 slab; E_{up} is the energy of the adsorbed system of CaO and Fe.

The calculated adsorption energies are shown in Fig. 4. All the values of E_{ads} are negative, indicating that adsorption happens in all three cases with different atom numbers of CaO. The absolute values of adsorption energy decrease with the increase of the atom number in the Ca–O system, suggesting favorable adsorption of CaO with a lower atom number. This calculation result well explains the different adsorption behaviors between CaO and Al_2O_3 shown in the in-situ experiment. For CaO with a smaller size, it is easier to be adsorbed by Al_2O_3 inclusions, which will increase the contact probability and thus the modification efficiency.

To further clarify the interaction between CaO and Al_2O_3 in this system, the adsorption behavior of the Ca atom was revealed with the assistance of electron density configurations. The chemical bonds around the Ca atom were analyzed

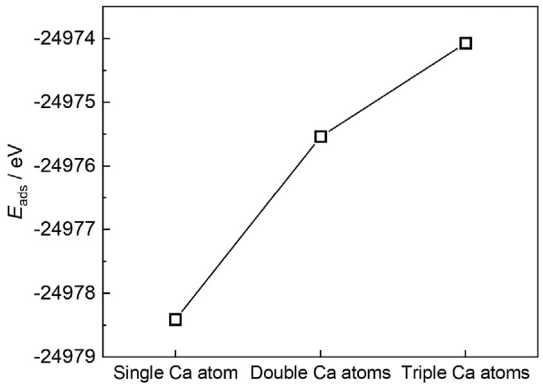

Fig. 4 – Adsorption energies between Al_2O_3 and CaO with different atom numbers.

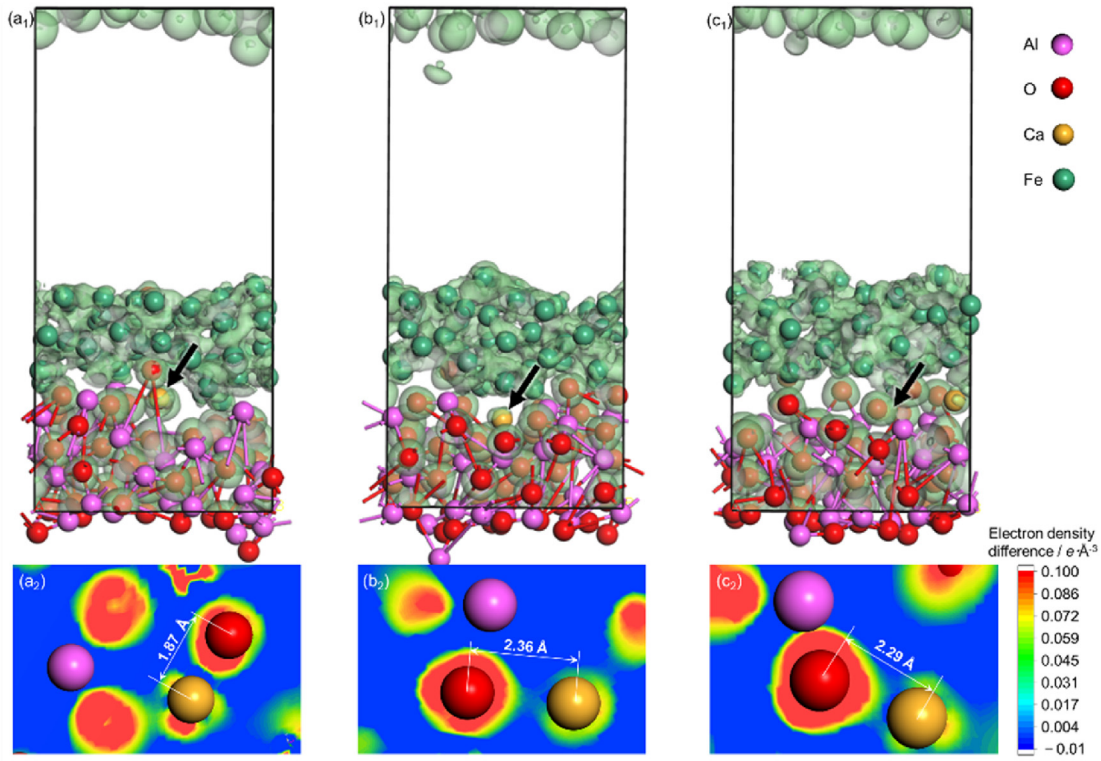

Fig. 5 – Electron density dispersion after adsorption with CaO of different atom numbers and the typical slices passing Ca and the nearest O and Al atoms: (a_1)-(a_2) single Ca atom (b_1)-(b_2) double Ca atoms (c_1)-(c_2) triple Ca atoms (the arrows point at the Ca atom showing in the corresponding slices).

accordingly. Fig. 5 shows the three-dimensional iso-surface plot of the electron density with a value of 0.025 e/Å^3 and the typical contours of electron density difference slices passing through the Ca atom and the nearest O and Al atom in the Al–O system. The color bar represents the valence electron redistribution due to adsorption. Obvious color differences can be observed along the Ca–O direction. Electron accumulates around O and depletes around Ca. Electron poor region adjacent to Ca atom with blue color can be found in all three cases. While there is no obvious charge difference along the Ca–Al direction, suggesting solid chemical bonds generate between Ca and O atom in Al–O system, which is consistent with the generation mechanism of Ca–Al–O inclusion in steel [9,24].

Population analysis was also adopted to illustrate the electron transfers and interaction between CaO and Al_2O_3 during the adsorption process. With Mulliken formalism, the projection of the plane wave states was analyzed based on a localized basis set. The overlapping populations and distances between the Ca atom and the nearest O/Al atom in the Al–O system are shown in Table 2. The values between Ca and O appear positive, while the values between Ca and Al are negative. A large positive value indicates the atoms are strongly bonded [25]. Therefore, the covalency in the bonds between Ca and O in the Al–O system is at high level. Furthermore, compared to the adsorption with double Ca atoms and triple Ca atoms, the adsorption and the chemical bond with single Ca atom is stronger due to the larger population. The distance between the Ca atom and the nearest O atom in the system with single Ca atom is also the smallest. Except for bonds between Ca and O, antibonding interactions between Ca and Al are also found in the systems with double Ca atoms and triple Ca atoms due to the negative overlapping population. The antibonding further reduces the interactions between CaO and Al_2O_3 in these two cases. Besides, the bonding phenomenon was also found between Fe atom and O atom in Al_2O_3 at the Fe/Al_2O_3 interface according to the bond population shown in Table 3. The bond lengths are around 1.73–2.02 Å, which is inconsistent with the structure of iron spinel reported in the existing literatures [26,27].

Table 2 – Bond population and the distances between Ca atom and the nearest O/Al atom in Al–O system.

System	Bond	Population	Distance/Å
Single Ca atom	Ca1–O48	0.18	1.87
Double Ca atoms	Ca1–O24	0.12	2.41
	Ca2–O45	0.09	2.36
	Ca2–Al25	−0.06	2.89
Triple Ca atoms	Ca1–O1	0.15	2.14
	Ca2–O26	0.1	2.43
	Ca3–O28	0.17	2.29
	Ca1–Al17	−0.07	2.97

Table 3 – Bond population and the distances between Fe atom and O atom in Al_2O_3 at the Fe/Al_2O_3 interface.

System	Bond	Population	Distance/Å
Single Ca atom	O4–Fe9	0.47	1.83
	O24Fe15	0.49	1.94
	O28–Fe53	0.59	1.74
	O48–Fe27	0.38	1.74
Double Ca atoms	O4–Fe49	0.47	1.73
	O24–Fe13	0.63	1.80
	O28–Fe55	0.4	1.94
Triple Ca atoms	O4–Fe47	0.59	1.97
	O24–Fe39	0.43	2.02
	O48–Fe36	0.49	1.87

4. Conclusions

In this study, a significant improvement of the adsorption ability of CaO particles on Al_2O_3 was found in liquid steel around 1550 °C due to the size effect. The adsorption behaviors and mechanisms were discovered in nano-scale with in-situ experiments and DFT calculations. The improvements appeared in terms of both faster adsorption speeds and stronger chemical bonds between Ca atom and O atom in the Al–O system when the size of CaO is smaller. The adsorption speed reaches 5.5 μm/s for CaO with a size of 2.2 μm, which is over twice for CaO with a size of 24.7 μm. The chemical bond between Ca and O in Al–O in the system with single Ca atom is proved to be the strongest with the assistance of electron density and bond population analysis. Furthermore, the surface of Al_2O_3 will become rough due to the chemical adsorption of CaO, encouraging more Ca atoms to participate in the adsorption and thus accelerating the adsorption process. The above discoveries provide new insight into the reactions concerning inclusion modification in liquid steel in nano-scale and also help create opportunities for the application of nanomaterials in high-efficient smelting.

Declaration of Competing Interest

The authors declare that they have no known competing financial interests or personal relationships that could have appeared to influence the work reported in this paper.

Acknowledgments

This work was financially supported by the Fundamental Research Funds for the Central Universities (No. FRF-TP-20-026A1) and the special grade of China Postdoctoral Science Foundation (No. 2021T140050).

REFERENCES

[1] Buffat P, Borel JP. Size effect on the melting temperature of gold particles. Phys Rev A 1976;13(6):2287–98.
[2] Rossnagel SM, Kuan TS. Alteration of Cu conductivity in the size effect regime. J Vac Sci Technol B 2004;22(1):240–7.
[3] Ji Y, Ma H, Su F, Wang G. Particle size effect on heat transfer performance in an oscillating heat pipe. Exp Therm Fluid Sci 2011;35(4):724–7.
[4] Xing L, Guo J, Li X, Zhang Z, Wang M, Bao Y, et al. Control of TiN precipitation behavior in titanium-containing micro-alloyed steel. Mater Today Commun 2020;25:101292.
[5] Liu W, Lian J, Münstermann S, Zeng C, Fang X. Prediction of crack formation in the progressive folding of square tubes during dynamic axial crushing. Int J Mech Sci 2020;176:105534.
[6] Zhao Y, Li T, Tang G, Guo H, Yan J, Guo X, et al. Characterization of the morphological evolution of MnS inclusions in free-cutting steel during heating. J Mater Res Technol 2022;17:1427–37.
[7] Chen S, Lei H, Hou H, Ding C, Zhang H, Zhao Y. Collision-coalescence among inclusions with bubble attachment and transport in molten steel of RH. J Mater Res Technol 2021;15:5141–50.
[8] Gu C, Bao Y-P, Gan P, Lian J-H, Münstermann S. An experimental study on the impact of deoxidation methods on the fatigue properties of bearing steels. Steel Res Int 2018;89(9):1800129.
[9] Zheng H-Y, Guo S-Q, Qiao M-R, Qin L-B, Zou X-J, Ren Z-M. Study on the modification of inclusions by Ca treatment in GCr18Mo bearing steel. Adv Manuf 2019;7(4):438–47.
[10] Webler BA, Pistorius PC. A review of steel processing considerations for oxide cleanliness. Metall Mater Trans B 2020;51(6):2437–52.
[11] Wang L, Song B, Yang Z-b, Cui X-k, Liu Z, Cheng W-s, et al. Effects of Mg and La on the evolution of inclusions and microstructure in Ca-Ti treated steel. International Journal of Minerals, Metallurgy and Materials 2021;28(12):1940–8.
[12] Sardar MK, Mukhopadhyay S, Bandopadhyay UK, Dhua SK. Optimisation of inclusion chemistry by improved steel cleanliness and optimum calcium treatment. Steel Res Int 2007;78(2):136–40.
[13] Deng Z, Zhu M. A new double calcium treatment method for clean steel refining. Steel Res Int 2013;84(6):519–25.
[14] Hu Y, Chen WQ, Han HB, Bai RJ. Influence of calcium treatment on cleanness and fatigue life of 60Si2MnA spring steel. Ironmak Steelmak 2017;44(1):28–35.
[15] Verma N, Pistorius PC, Fruehan RJ, Potter M, Lind M, Story SR. Transient inclusion evolution during modification of alumina inclusions by calcium in liquid steel: Part II. Results and discussion. Metall Mater Trans B 2011;42(4):720–9.
[16] Visser H-J, Boom R. Advanced process modelling of hot metal desulphurisation by injection of Mg and CaO. ISIJ Int 2006;46(12):1771–7.
[17] Wang X, Tang F, Li Z, Tian Y, Meng J, Zhu M, et al. Development of a high-efficiency dephosphorization process via the fine in situ phases due to the composite ball explosion. Ironmak Steelmak 2021;48(9):1110–4.
[18] Wang X, Tang F, Li Z, Tian Y, Meng J, Zhu M, et al. Desulphurisation with dispersed in-situ phases induced by composite ball explosive reaction during ultra-low carbon steel production in RH degasser. Ironmak Steelmak 2022;49(2):217–25.
[19] Payne MC, Teter MP, Allan DC, Arias TA, Joannopoulos JD. Iterative minimization techniques for ab initio total-energy calculations: molecular dynamics and conjugate gradients. Rev Mod Phys 1992;64(4):1045–97.
[20] Perdew JP, Chevary JA, Vosko SH, Jackson KA, Pederson MR, Singh DJ, et al. Erratum: atoms, molecules, solids, and surfaces: applications of the generalized gradient approximation for exchange and correlation. Phys Rev B 1993;48(7). 4978-4978.
[21] Vanderbilt D. Soft self-consistent pseudopotentials in a generalized eigenvalue formalism. Phys Rev B 1990;41(11):7892–5.

[22] Chen Y, Ouyang C, Shi S, Sun Z, Song L. Density functional theory study of Ir atom deposited on γ-Al_2O_3 (001) surface. Phys Lett 2009;373(2):277–81.
[23] Digne M, Sautet P, Raybaud P, Euzen P, Toulhoat H. Use of DFT to achieve a rational understanding of acid–basic properties of γ-alumina surfaces. J Catal 2004;226(1):54–68.
[24] Costa e Silva ALVd. Non-metallic inclusions in steels – origin and control. J Mater Res Technol 2018;7(3):283–99.
[25] Hu Q, Wu Q, Sun G, Luo X, Liu Z, Xu B, et al. First-principles study of atomic oxygen adsorption on boron-substituted graphite. Surf Sci 2008;602(1):37–45.
[26] Li L, Gan Y-M, Lu Z-H, Xiaohu Y, Qing S, Gao Z, et al. The effects of Fe, Co and Ni doping in CuAl2O4 spinel surface and bulk: a DFT study. Appl Surf Sci 2020;521:146478.
[27] Shi L, Meng S, Jungsuttiwong S, Namuangruk S, Lu Z-H, Li L, et al. High coverage H2O adsorption on CuAl2O4 surface: a DFT study. Appl Surf Sci 2020;507:145162.